Bimolecular $Ni^+(^2D_{5/2}) + C_3H_8$ Reaction Dynamics in Real Time

Robert J. Noll, Sung Soo Yi, and James C. Weisshaar*

Department of Chemistry, University of Wisconsin—Madison, Madison, Wisconsin 53706-1396

Received: August 13, 1997; In Final Form: October 21, 1997[⊗]

A beam of $Ni^+(^2D_{5/2})$ is formed at a sharp zero of time by resonant two-photon ionization with a nanosecond dye laser pulse and crossed with a beam of propane gas under single-collision conditions at collision energies of 0.01 and 0.21 eV. The ion−molecule reaction occurs in field-free space in the extraction region of a time-of-flight mass spectrometer. After a variable time delay $t_{ext} = 1-8$ μs, a fast high-voltage pulse extracts product ions and residual reactant ions into a field-free flight tube for mass analysis. In contrast with many earlier studies of this reaction under more energetic conditions, at 0.01 eV collision energy we find that $Ni^+(^2D_{5/2})$ reacts with C_3H_8 to form long-lived $NiC_3H_8^+$ complexes almost exclusively (≥96%) on the time scale 0−25 μs after initiation of the collision. Retarding field analysis of the decay of the long-lived $NiC_3H_8^+$ complexes reveals that on a 6−24 μs time scale 28% revert to $Ni^+ + C_3H_8$ and 6% form $NiC_2H_4^+ + CH_4$ elimination products; the remaining complexes have not yet decayed at $t = 25$ μs. At 0.21 eV collision energy, both CH_4 and H_2 elimination products are formed promptly (in less than 1 μs) and also over the entire range of time scales studied, 0.5−25 μs. Even at this higher collision energy, about 25% of the long-lived complexes survive beyond $t = 25$ μs. The apparent energetic threshold observed here for the first time provides new evidence of a potential energy barrier to elimination products comparable to the energy of ground-state reactants. In addition, direct measurement of the *time scale* of the reaction under carefully controlled conditions provides new dynamical information that serves as a benchmark for the theoretical treatment presented in the accompanying paper.

I. Introduction

Reactions of gas-phase transition-metal atoms can serve as useful model systems for the purpose of calibrating theoretical methods for the treatment of complex organometallic reactions. The rich gas-phase chemistry of atomic metal cations (M^+)[1] and of neutral metal atoms (M)[2] has been studied extensively over the past 15 years. From a theoretical viewpoint,[3] these reactions provide a relevant degree of electronic complexity (due to the presence of open d-subshells and many low-lying electronic states) without the additional burden of ligands and solvent present in condensed-phase chemistry. By careful control of initial M^+ electronic state and of collision energy, increasingly sophisticated experiments are providing ever more stringent tests of the ability of approximate electronic structure theories to produce accurate potential energy surfaces along key reaction paths. Theory in turn is providing a new level of mechanistic detail, sometimes corroborating and sometimes disputing earlier speculation about the detailed nature of reaction intermediates and transition states.

A particularly well-studied set of reactions involves the dehydrogenation and demethanation of propane in collisions with the late 3d-series cations Fe^+, Co^+, and Ni^+.[4−17] The early observations of exothermic H_2 and CH_4 elimination products indicative of CH and CC bond activation at low collision energy were quite surprising in view of the difficulty of carrying out analogous bond activation steps in solution phase. A long series of studies employing ion beams,[4−7,11,13,16,17] fast flow reactors,[10] ion cyclotron resonance mass spectrometers,[8,9] and tandem mass spectrometers[12,14−16] have been aimed at determining the energetics of different reaction steps, the nature of important pathways to H_2 and CH_4 elimination, and the effects of kinetic energy, initial M^+ electron configuration and spin, and isotopic substitution on reaction probability and product branching. Most recently, new electronic structure theories[18] have been brought to bear on these same reactions, providing a new level of mechanistic detail. The emerging picture is complicated. It is likely that initial insertion of M^+ into a CH bond leads to H_2 elimination, but we still are not certain whether CH_4 elimination occurs via initial CH or CC bond insertion.[14,16,17] In addition, theory strongly suggests[18] that earlier postulated stepwise mechanisms[14,16] should be replaced by more concerted motions involving fewer potential minima, as we will discuss in detail in the accompanying paper 2.[19]

In the present experimental work, we study the reaction of ground-state Ni^+ ($^2D_{5/2}$) with propane at collision energies of 0.01 eV (0.2 kcal/mol) and 0.21 eV (4.8 kcal/mol) under carefully controlled, single-collision, crossed-beam conditions.[20−22] The state-specific Ni^+ beam is formed at a sharp zero of time by resonant two-photon ionization (R2PI) using a nanosecond dye laser. The subsequent formation of long-lived $NiC_3H_8^+$ complexes (1a) and their evolution back to Ni^+ reactants and forward to CH_4 and H_2 elimination products (1b, 1c) is monitored *in real time* with roughly 0.5 μs resolution using pulsed time-of-flight mass spectrometry (TOF-MS). Long-lived complexes that survive extraction may fragment in the field-free flight tube; we can further analyze the dynamics by using retarding fields[23] to separate these fragments.

* To whom correspondence should be addressed. E-mail addresses weisshaar@chem.wisc.edu.

⊗ Abstract published in *Advance ACS Abstracts,* December 15, 1997.

S1089-5639(97)02673-X CCC: $15.00
Published on Web 01/08/1998

$$Ni^+ + C_3H_8 \rightarrow \begin{cases} NiC_3H_8^+ & (1a) \\ NiC_2H_4^+ + CH_4 & (1b) \\ NiC_3H_6^+ + H_2 & (1c) \end{cases}$$

The result is a set of *time-resolved branching fractions* measured under carefully controlled reaction conditions. These provide a new benchmark for comparison with theoretical work. In the accompanying paper 2, we present electronic structure calculations on the energetics of potential wells and transition states for the same $Ni^+ + C_3H_8$ reaction. We will use those results, including moments of inertia and vibrational frequencies, to build a realistic, comprehensive rate model of the reaction. The dynamics are treated using statistical rate theory (RRKM theory) on a single adiabatic potential energy surface.[24] We will find that moderate adjustments of the energetic parameters from theory bring the rate calculations into good agreement with our experimental data and many others, including cross sections vs kinetic energy, elimination branching fractions, and H/D isotope effects. The combination of theory and experiment thus elevates our fundamental understanding of this reaction to a new level of sophistication.

II. Experimental Section

A. Crossed-Beam Measurements. The crossed-beam apparatus (Figure 1) and its usual operating parameters have been described previously.[20−22] In the source chamber, gas-phase nickel atoms are produced in a laser ablation source[25] and seeded into an argon beam, which is skimmed and collimated. Electric fields strip ions from the beam. In the interaction chamber, the nickel atoms are ionized by a pulsed dye laser, initiating bimolecular ion−molecule collisions. The Ni^+ cations react in field-free space with hydrocarbon molecules from a second pulsed valve. After a suitable reaction delay, a high-voltage pulse extracts reactant and product ions into the time-of-flight mass spectrometer (TOF/MS) for analysis.

The frequency-doubled dye laser (10 ns fwhm, 323.384 nm, <250 μJ/pulse) intersects the atomic beam and resonantly photoionizes Ni via the $z^3G_5^0 \leftarrow \alpha_3F_4$ transition at 30 923 cm^{-1}.[26] Absorption of two such photons creates Ni^+ exclusively in the $^2D_{5/2}$ state. The two-photon energy is only 227 cm^{-1} above the ionization energy of 61 619 cm^{-1}.[27] The nearest Ni^+ excited state is $^2D_{3/2}$ at 1507 cm^{-1} above the IE. A log−log plot of Ni^+ ion yield vs laser pulse energy is linear with slope of unity, consistent with a two-photon process whose first step is saturated. The metal ion velocity is that of the neutral beam, $(5.8 \pm 0.5) \times 10^4$ cm/s.[22]

The packet of Ni^+ (1000−8000 ions/shot) intersects the beam of hydrocarbon molecules in the extraction region of a Wiley−McLaren time-of-flight mass spectrometer (TOF-MS).[28] Neat propane gas (Matheson, >99.9% purity) expands from a second 0.5 mm pulsed nozzle; the propane beam is pseudoskimmed (i.e., not differentially pumped) by a set of home-built rectangular knife edges. The propane velocity is $(7.6 \pm 1.0) \times 10^4$ cm/s.[22] The typical propane pressure behind the nozzle is 60 Torr. From the work of Fenn and co-workers,[29] we estimate that the propane is cooled to a vibrational temperature of about 50 K. Plots of product yield vs hydrocarbon backing pressure are linear from 10 to 120 Torr, indicating that single-collision conditions obtain at 60 Torr.

By changing the angle between the Ni^+ and propane beams, we can vary the collision energy in coarse steps. We have conducted the experiments at two such geometries, 20° and 145°. The corresponding collision energies are 0.011 ± 0.010 eV (0.25 ± 0.23 kcal/mol) and 0.21 ± 0.09 eV (4.8 ± 2.1 kcal/mol).

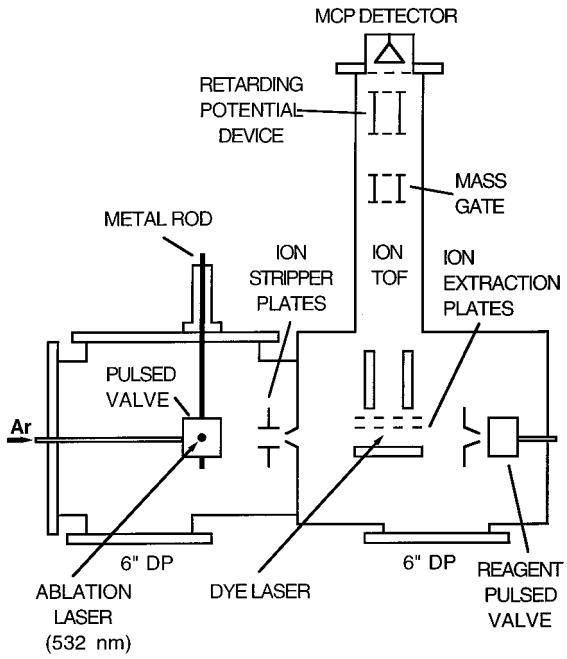

Figure 1. Schematic of ion−molecule crossed beam apparatus.

The estimated uncertainties reflect worst-case analyses accounting for uncertainties in the metal and hydrocarbon velocities, small additional velocity imparted to the metal ions by space charge effects, and the range of angles of intersection of the two velocity vectors. The larger collision energy is better defined. We refer to the smaller energy as "nominal 0.01 eV"; we believe it includes a distribution of energies peaked at 0.01 eV and lying below 0.02 eV = 0.5 kcal/mol. The two energy distributions do not overlap.

The 10 ns laser pulse initiates ion−molecule collisions at a sharply defined starting time. After a variable delay time that allows collisions to occur, reactant and product ions are extracted at time t_{ext} into the TOF-MS for analysis. We can obtain useful signals for extraction times in the range $0.2\ \mu s \le t_{ext} \le 8\ \mu s$. At t_{ext}, high-voltage pulses (1−1.5 kV) are applied to the ion extraction plates, sending reactant and product ions toward the detector. The voltage pulses rise to 90% of their plateau values in 20 ns; the analogous rise time of the electric field in the first extraction region is about 13 ns. The mass resolution ($m/\Delta m$) is >250 for products near 100 amu. Plots of TOF vs $m^{1/2}$ are linear to within 3 ns (rms) residuals, sufficient for unambiguous mass assignments. Ions are detected with a microchannel plate (Galileo FTD-2003) operated at 6×10^7 gain. Detector output is 50 Ω coupled to a LeCroy 9400 digital oscilloscope without further amplification. We estimate detector mass discrimination effects at less than 10%.[30] Since the detector dynamic range cannot simultaneously accommodate Ni^+ and product ion signal, a small set of electrodes mounted in the drift region—labeled "mass gate" in Figure 1—is pulsed at the appropriate time to deflect Ni^+ ions away from the detector.[22]

Mass spectra are complicated by the presence of five Ni isotopes at 58 amu (68%), 60 amu (26%), 61 amu (1.3%), 62 amu (3.7%), and 64 amu (1.2%). Quantitative product branching ratios are based on the areas under well-resolved peaks, usually of the majority isotope (^{58}Ni) for product peaks. In cases of mass interferences, areas of blended peaks were scaled to the ^{58}Ni basis using published Ni isotope abundances.[31] For example, adduct ion abundances were measured by integrating the $m = 102$ peak ($^{58}NiC_3H_8^+ + {}^{60}NiC_3H_6^+$) and correcting for the $^{60}NiC_3H_6^+$ contribution.

Under single-collision conditions, total product signal should rise linearly with Ni^+ number density, hydrocarbon number density, and t_{ext}, which we have experimentally verified. Moreover, the reaction should be insensitive to argon backing pressure. We have run the experiment at twice and half the normal argon backing pressure of 1.7 atm with $t_{ext} = 8$ μs and observe no changes in branching fractions or product yield relative to Ni^+.

As unreacted Ni^+ ions are extracted, they accelerate through the hydrocarbon cloud in the interaction region and can form higher-energy reaction products. By applying the HV extraction pulses before the laser fires, this contribution to the total reaction products can be measured. The background contribution is constant, so it should be more prominent at shorter t_{ext}. Although unimportant (2−3%) at $t_{ext} = 8$ μs, background products become about 15% of the products at $t_{ext} = 1.1$ μs and about 25−50% of the products at $t_{ext} = 300$ ns. Here "products" include both intact complexes and elimination products (channels 1a, 1b, and 1c). Complexes from such background collisions are formed from a broad distribution of collision energies peaked at low energy but effectively extending up to several electronvolts, beyond which the Langevin cross section rapidly diminishes the collision probability. Thus background products favor higher energy processes. Accordingly, we find about $^2/_3$ elimination products and $^1/_3$ adducts in the background mass spectrum.

It is important to distinguish clearly two different time scales that we will refer to frequently. The first, which we have already called t_{ext}, is the experimental time window during which the Ni^+ and C_3H_8 reactant beams are "in contact" and collisions at a well-defined energy may occur. This is the time between the ionizing laser pulse and the ion extraction pulse. The second time, which we simply call t, refers to the time since a long-lived complex was formed in a bimolecular collision. It is the sort of time that will appear naturally in paper 2 in a kinetics model for the unimolecular decay of a population of $Ni^+(C_3H_8)$ complexes *which were all present at* $t = 0$. Because our experiment is firmly in the single-collision limit, to a very good approximation we create collision complexes with a uniform distribution of initiation times over a time window of width t_{ext}. When we sample the fate of this collection of complexes at a particular real experimental time after the ionizing laser pulse, we sample complexes that have evolved over a corresponding distribution of times t after initiation. In comparing kinetics models with experiment, we will properly average over this distribution.

B. Analysis of Metastable Decay by Retarding Potential Method. Under our carefully controlled reaction conditions, the product mass spectra reveal an abundance of long-lived $NiC_3H_8^+$ collision complexes (1a). These complexes have survived extraction intact, since they arrive at the detector at appropriate times for such adduct ions. The time during which $NiC_3H_8^+$ is accelerated by the extraction fields is about 2 μs. Under our single-collision conditions, the complexes are metastable. They have sufficient energy to fragment either to $Ni^+ + C_3H_8$ reactants or to exothermic $NiC_2H_4^+ + CH_4$ (1b) or $NiC_3H_6^+ + H_2$ (1c) elimination products. For $t_{ext} = 8$ μs, complexes that survive $t = 2-25$ μs after they are formed will fragment in the field-free drift region of the mass spectrometer.

Such metastable decay can be analyzed by applying a retarding potential in the flight tube between the reaction zone and the detector (Figure 1).[23] In the retarding potential device (Figure 2), a series of four metal meshes establish a region of variable positive potential with respect to ground (the flight tube

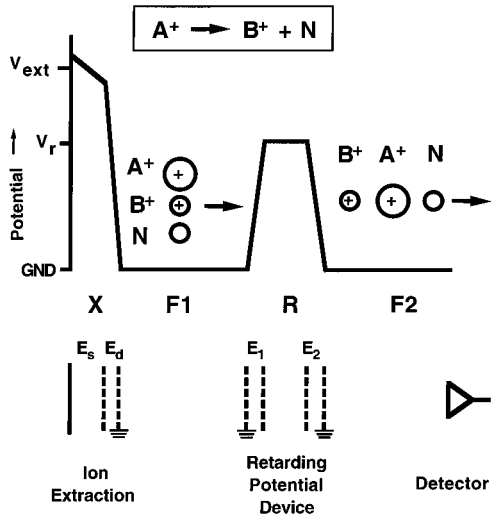

Figure 2. Bottom: schematic of ion flight path including retarding potential device. Top: schematic of changes in potential energy along flight path. Retarding device separates metastable adduct ions (A^+) from fragment ions (B^+) and corresponding neutrals (N), all of which are detected.

potential). After extraction, an ion approaching from the first field-free region (F1, Figure 2) enters the decelerating field E_1 and slows down. It traverses the ion retarding region (R) at constant, but diminished velocity. In the accelerating field E_2, it recovers its original velocity. It then passes into a final 13 cm long field-free region (F2) before striking the detector. The retarding device is 11 cm long and lies 85−96 cm above the extraction region, near the end of the ion flight path whose entire length is 109 cm. A 10 cm stainless steel tube floats at the retarding potential V_r; its ends are covered by nickel mesh (70 lines/in., 85% optical transmission, Buckbee-Mears, St. Paul, MN). On either end of the tube, an additional electrically isolated, grounded mesh is mounted 0.54 cm from the end. The rest of the flight tube is shielded from the high voltage of the floating tube by the end meshes and additional grounded metal sheet. The device is described in additional detail elsewhere.[22]

As compared with the usual time-of-flight mass spectrometer, the retarding potential device alters arrival times in a mass-dependent fashion. In the examples presented below, we are able to distinguish long-lived $NiC_3H_8^+$ complexes that survive the entire flight path intact, complexes that fragment in region F1 before entering the retarding field, and complexes that fragment in the retarding device, region R. Neutral fragments formed in F1 also create a distinguishable peak whose arrival time is insensitive to V_r.

III. Results

A. Simple Time-of-Flight Mass Spectra. In Figure 3, we show product time-of-flight mass spectra recorded at nominal 0.01 eV and at 0.21 eV collision energy with $t_{ext} = 8$ μs. At the lower collision energy, the dominant product (96 ± 1%) is the long-lived complex $NiC_3H_8^+$ (1a). We also see 3 ± 1% of the CH_4 elimination product, $NiC_2H_4^+$ (1b), and 0.7 ± 0.4% of the H_2 elimination product, $NiC_3H_6^+$ (1c). The latter can be cleanly observed without interference from adduct ions only for the ^{58}Ni isotope. At nominal 0.01 eV collision energy, we estimate that the total reaction cross section (to form all observed products, both adducts and elimination products) is 260 ± 80 Å,^{2} 65 ± 30% of the Langevin cross section[32] of 390 Å^2 at 0.01 eV. For $t_{ext} = 8$ μs, only a small fraction (≤3%) of the total product ions including adducts are due to background

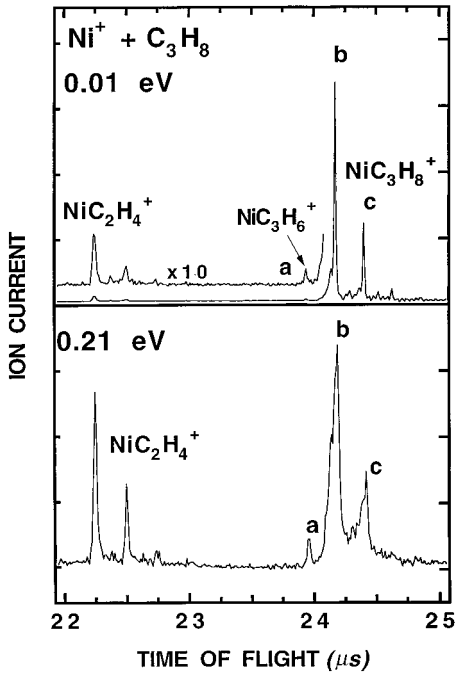

Figure 3. Product region of time-of-flight mass spectra for $t_{ext} = 8$ μs, collision energy $E_t = 0.01$ eV (nominal, top trace) and 0.21 eV (lower trace). Peak a is $^{58}NiC_3H_6^+$ from H_2 elimination, peak c is $^{60}NiC_3H_8^+$ adduct, and peak b is a blend of $^{58}NiC_3H_8^+$ and $^{60}NiC_3H_6^+$.

reaction of fast Ni^+ during extraction, as described above. For shorter reaction times between 0.2 and 1 μs (not shown), $NiC_2H_4^+$ accounts for about 7% and $NiC_3H_6^+$ for about 2% of total products. This difference in branching at shorter extraction times is probably due to the larger relative importance of high-energy collisions from background reactions, rather than a dramatic time dependence of the product branching at 0.01 eV collision energy. It is *possible* that the very small fraction of prompt elimination products observed at nominal 0.01 eV collision energy arises entirely from the high-energy range of the distribution (near 0.02 eV) or from the high-energy collisions that occur during ion extraction. The modeling in paper 2 suggests that this is so.

At the higher collision energy of 0.21 eV and $t_{ext} = 8$ μs (Figure 3, bottom) we observe the same three product ions but with elimination products in much higher proportion. The branching fractions are 23 ± 4% $NiC_2H_4^+ + CH_4$, 4 ± 2% $NiC_3H_6^+ + H_2$, and 73 ± 4% $NiC_3H_8^+$, constant within experimental uncertainty for t_{ext} between 1 and 8 μs. As t_{ext} decreases below 1 μs, $NiC_2H_4^+$ accounts for as much as 35%, and $NiC_3H_6^+$ for as much as 11%, of all products. Again, the increase in elimination products at shorter t_{ext} is probably due to background reactions of accelerated Ni^+ ions during extraction. The absolute reaction efficiency was not measured for this collision energy, but it is comparable to that at the lower energy.

The prompt product branching fractions measured for $t_{ext} = 8$ μs, including adducts, are summarized for the two collision energies in Table 1. In Table 2, we compare the branching between the two elimination products under our conditions with that observed in earlier work using a variety of techniques. With two exceptions, the fraction of CH_4 elimination products lies in the range 80−85%, indicating that the *branching* is rather insensitive to differences in collision energy and internal electronic and vibrational energy of $Ni^+ + C_3H_8$ reactants.

The $NiC_3H_8^+$ adduct peaks in Figure 3 are clearly broadened compared to the prompt elimination product peaks. The

TABLE 1: Branching Fractions Including Complexes, t = 2−10 μs after Collision[a]

E_t (eV)	$NiC_2H_4^+$	$NiC_3H_6^+$	$NiC_3H_8^+$
0.01	3 ± 1	0.7 ± 0.4	96 ± 1
0.21	23 ± 4	4 ± 2	73 ± 4

[a] Data for $t_{ext} = 8$ μs, $U_{ext} = 1280$ eV, which places the time since initiation of $Ni^+ + C_3H_8$ collisions in the range 2−10 μs.

TABLE 2: Comparison of Elimination Product Branching Fractions

E_t (eV)	technique[a]	$NiC_2H_4^+ + CH_4$	$NiC_3H_6^+ + H_2$	ref
0.01	CB	81	19	this work
0.21	CB	85	15	this work
∼1	IB+G	80	20	5
∼0.5	IB+G	67	33	6, 7
<1	IB+G	78	22	11
0.05	IB+G	80	20	16
TE[b]	ICR	83	17	6
TE	ICR	80	20	8, 9
TE	FR	85	15	10
TE	TMS	64	36	16

[a] CB = crossed beams; IB+G = ion beam plus gas cell; ICR = ion cyclotron resonance; FR = flow reactor at 0.75 Torr of He buffer; TMS = tandem mass spectrometry. [b] Thermal energy distributions near 300 K.

broadening is especially evident at 0.21 eV, where the peaks have tails toward shorter TOF. At nominal 0.01 eV, a small, partially resolved peak toward shorter arrival time is just visible as well. This broadening and tailing occur in the simple TOF mass spectra because some collision complexes have fragmented in the drift region of the mass spectrometer. Release of kinetic energy into fragments might explain a symmetric broadening of the adduct peaks, but we believe this is a minor effect under our extraction conditions. Instead, the strong electric field at the detector, 1300 V/cm acting over only the last 2 cm of the flight path, causes the asymmetric tailing toward shorter TOF. The lighter fragment ions suffer a larger acceleration than the intact adduct ions and thus arrive slightly earlier in time. Parents and fragments are only partially resolved by this final field. Decreasing the ion extraction energy (and hence, increasing the TOF to the detector) increases the apparent relative size of the tail by improving the resolution of parent and fragments. Varying t_{ext} changes the total number of product ions but not the general appearance of the adduct peaks.

Fast *neutral* fragments born in the field-free region, mostly C_3H_8, are detected only 10−20% as efficiently as cations, but they also contribute to the peak shape, especially at 0.21 eV. Since neutral fragments are not accelerated by the final electric field near the detector, they arrive at slightly *longer* times than the intact adduct ions. These neutrals cause the low-intensity tail seen at the far right of Figure 3, as explained below.

Finally, we mention in passing that we have preliminary results at a higher collision energy $E = 0.7$ eV using He as the carrier gas for the Ni beam.[33] In this case, CH_4 elimination accounts for 85% and H_2 elimination for 15% of the products, i.e., *no adducts are observed*.

B. Retarding Field Analysis of Delayed Complex Fragmentation. *1. Mass Spectra vs Retarding Potential.* The purpose of the retarding field measurements is to separate all $NiC_3H_8^+$ complexes that survive extraction into two groups, those that fragment at $t \leq 25$ μs and those that do not. We can also measure the branching among the delayed fragmentation channels. In Figure 4 product mass spectra (0.21 eV collision energy, $t_{ext} = 8$ μs) are shown as a function of the voltage V_r

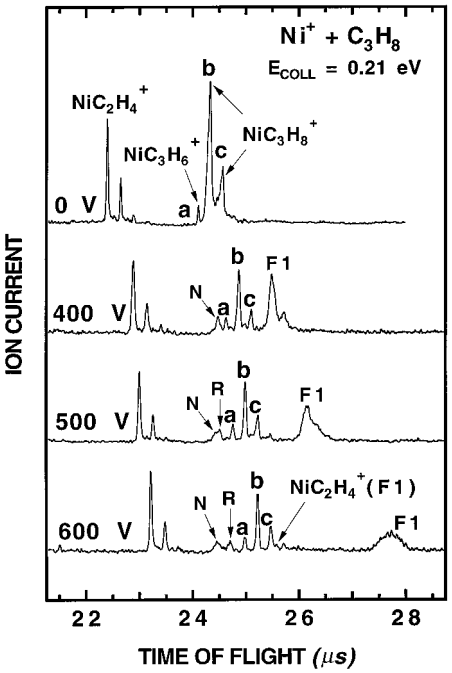

Figure 4. Time-of-flight mass spectra vs retarding field voltage V_r (see text) using $t_{ext} = 8$ μs and $E_t = 0.21$ eV. Peaks a, b, and c are the same peaks described in Figure 3. N labels neutral fragments. R and F1 label Ni^+ fragments born in segments R and F1 of Figure 2.

applied to the retarding field device of Figure 2. The ion extraction energy is 1280 eV. The spectrum at $V_r = 0$ again shows the sharp peaks due to prompt CH_4 and H_2 elimination products formed before ion extraction and the broader adduct ion peaks with substantial tailing. As V_r increases, the entire mass spectrum moves toward longer arrival times due to the slower transit of all ions through the retarding region. We label the large, sharp peaks due to the two dominant isotopes of prompt $NiC_3H_6^+ + H_2$ products and intact $NiC_3H_8^+$ adducts as a, b, and c on all spectra. A large new peak gradually emerges to the right of a, b, c; at $V_r = 400$ V it is resolved as a doublet. The analysis below identifies the doublet as atomic Ni^+ isotopes arising from fragmentation of $NiC_3H_8^+$ in region F1 of the flight tube, prior to the retarding field (Figure 2). At the highest retarding voltage shown, $V_r = 600$ V, we barely observe a very small peak to the right of peak *c* that is assigned to $NiC_2H_4^+$ ($+CH_4$) formed in region F1. We do not observe a peak arising from delayed fragmentation to $NiC_3H_6^+$ ($+H_2$), evidently because the fragmentation branching into this channel is too small. A set of much smaller peaks emerges to the left of peak a; these are due to Ni^+ fragments born in region R. They are decelerated by the first field E_1 as $NiC_3H_8^+$ but accelerated by E_2 as lighter Ni^+ fragments. They emerge from the retarding device at *higher* speed than intact adducts and thus arrive at the detector slightly earlier.

We have acquired similar retarding field mass spectra at the lower collision energy of 0.01 eV. They are qualitatively the same as the 0.21 eV spectra but of lower signal-to-noise ratio since far fewer of the adducts fragment at 0.01 eV. In particular, $Ni^+ + C_3H_8$ again dominates the delayed fragments.

When fragmentation to $Ni^+ + C_3H_8$ occurs in region F1, the lighter Ni^+ ions have less kinetic energy than the intact adducts, simply because they have the same speed but less mass. For example, $^{58}Ni^+$(F1) fragments have only 57% of the kinetic energy of their $^{58}NiC_3H_8^+$ parents. For an extraction energy of 1280 eV, this is only 730 eV. Thus, $V_r = 600$ V in Figure 4 is approaching the stopping potential for Ni^+(F1) fragments. They are delayed toward infinite arrival time as V_r approaches the stopping potential.

Peaks due to prompt product ions (including intact adducts) and delayed fragments have different widths in Figure 4 because the Wiley−McLaren space-focusing condition[28] cannot be maintained for both types of ion. Application of the retarding voltage V_r increases ion arrival times, in effect "lengthening" the flight tube. If the ion extraction fields are tuned to make a sharp mass spectrum for prompt ions with $V_r = 0$, these same ions go out of space focus as V_r increases. To avoid this broadening, in the mass spectra of Figure 4 we have chosen to slightly alter the ratio of extraction fields to maintain good space focus of the prompt elimination products and the intact $NiC_3H_8^+$ peaks, including peaks a, b, and c. This changes the ion extraction energy very little, by less than 8 eV out of 1280 eV. The peaks due to delayed Ni^+ fragment peaks born in region F1 then necessarily broaden, since they were extracted as $NiC_3H_8^+$ but traverse region R as Ni^+. The peaks due to delayed Ni^+ fragments born in region R remain quite sharp since they are extracted as $NiC_3H_8^+$, traverse region R at the appropriate velocity for adducts, and can go out of space focus only in the relatively short region F2.

2. Calibration and Assignment of Peaks. In describing the process of assigning fragment masses, it is convenient to adopt a compact notation that describes in which region of the apparatus each type of fragment ion was born. These are the ion extraction region X, the first field-free region F1, the ion retarding region R, and the second field-free region F2, as shown in Figure 2. For example, we denote Ni^+ fragments born in the first field-free region Ni^+(F1); those born in the retarding region are Ni^+(R). Neutral fragments, which we cannot identify by mass, are N(F1) and N(F2). Since most of the ionic fragments prove to be Ni^+, most of the neutral fragments are evidently C_3H_8. Prompt elimination products born in the ion extraction region X are denoted $NiC_3H_6^+$(X) and $NiC_2H_4^+$(X). Long-lived adduct ions that survive to the detector intact are simply denoted $NiC_3H_8^+$.

In our one-dimensional model of the apparatus, the ion extraction energy U_{ext} (typically near 1280 eV) is adjusted slightly to best fit arrival times of $NiC_3H_6^+$(X), $NiC_2H_4^+$(X), and $NiC_3H_8^+$ in a least-squares sense. The lengths of regions F1, R, and F2 are the physical lengths 85, 10, and 13 cm, respectively. We assume no fragmentation in the short regions of the decelerating and accelerating electric fields E_1 and E_2. The retarding potential $V_r = 400-800$ V and the decelerating and accelerating electric fields E_1 and E_2 are all measured quantities. We model the detector region approximately by including a constant electric field $E_{det} = 1300$ V/cm in the last 2 cm of flight to the detector plane.

It is then straightforward to write the flight time of intact adducts, prompt elimination products, and delayed ion and neutral fragments born in region F1 or region R as a sum of transit times through each region of piecewise constant electric field in the apparatus. In practice, for the most direct comparison with experiment we calculate the *change* in TOF, $\Delta(\text{TOF}) = \text{TOF}(V_r) - \text{TOF}(V_r = 0)$, for each type of particle as a function of V_r. For fragments, $\text{TOF}(V_r = 0)$ is defined as the arrival time of intact adducts, peak b in Figure 4. Each contribution to Δ(TOF) can be calculated from simple one-dimensional classical mechanics, taking proper account of possible changes in mass and kinetic energy due to fragmentation in the prior region. The model neglects kinetic energy

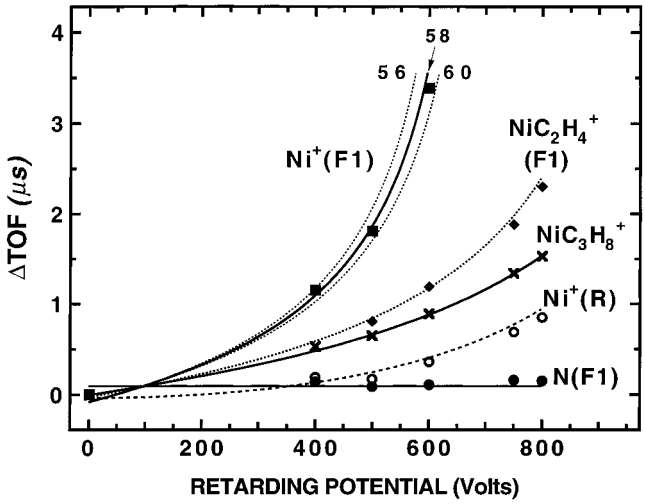

Figure 5. Change in flight time for different peaks in Figure 4 with retarding voltage turned on vs off, plotted vs the retarding potential V_r. Lines are calculated from the model of the flight tube as described in the text. For the $^{58}Ni^+(F1)$ peak, the two dashed lines show the sensitivity to changes of ±2 amu in the assumed mass of the fragment.

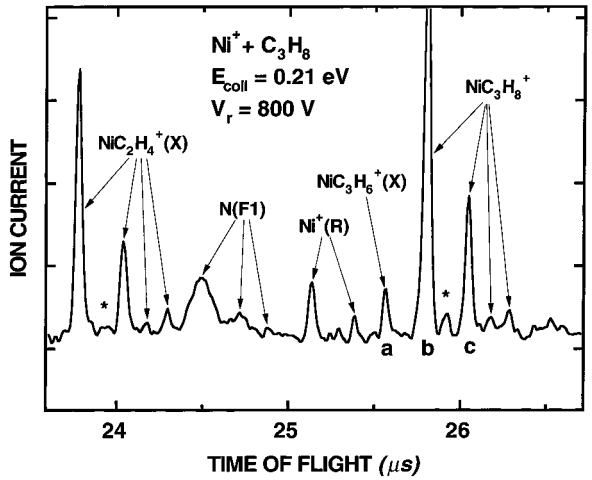

Figure 6. Assignment of details of time-of-flight mass spectrum with $V_r = 800$ V, near the stopping potential for $Ni^+(F1)$ fragments. Asterisks mark peaks probably due to $Ni^{13}C_3H_8^+$ isotopomer. The assignments are based on the fits shown in Figure 5.

release on fragmentation and the slight change in U_{ext} due to readjustment of the Wiley−McLaren space focusing fields at each V_r.

Figure 5 compares observed and calculated Δ(TOF) vs V_r for a typical set of data with $U_{ext} = 1280$ eV and $V_r = 0-800$ V. All plots are for the predominant ^{58}Ni isotope peaks. Arrival times are measured as intensity maxima. The fits to the fragment peaks $Ni^+(F1)$ and $NiC_2H_4^+(F1)$ are very good. The computed Δ(TOF) for region F1 fragment ions depends primarily on the model within the retarding field device and near the detector. The family of curves plotted for $Ni^+(F1)$ using the mass 56, 58, or 60 amu shows the sensitivity of the calculated Δ(TOF) to the assumed mass of the fragment. We can easily assign region F1 fragment masses within ±2 amu, more than adequate to unambiguously assign the $Ni^+(F1)$ and $NiC_2H_4^+(F1)$ peaks. The model is somewhat less successful in fitting fragment ions born in region R, as witness the $Ni^+(R)$ curve. These Δ(TOF) depend on the modeling not only in the retarding field device but also in region F2 and in the detector region. Again, however, Δ(TOF) is extremely sensitive to changes in the assumed mass of region R fragments. A change of 2 amu in the assumed $Ni^+(R)$ mass shifts the calculated curve by twice the difference between experimental and calculated curves in Figure 5. Thus we can identify the region R fragment peaks unambiguously as $Ni^+(R)$. The broad peak due to neutral fragments, primarily $C_3H_8(F1)$, is also well fit by the model.

With the masses and processes leading to each peak firmly assigned, we can account for essentially all of the little peaks that emerge with increasing V_r. Figure 6 shows the feasible level of detail for peak assignments at $V_r = 800$ V (not shown in Figure 4). The $Ni^+(F1)$ fragments have been stopped in the retarding device at this voltage. From left to right, we can resolve (at least partially) and identify region F1 neutral fragments (primarily C_3H_8) that were originally extracted as $^{58}NiC_3H_8^+$ and $^{60}NiC_3H_8^+$ complexes, and perhaps $^{62}NiC_3H_8^+$ as well; the same three isotopes for region R ionic fragments $Ni^+(R)$; prompt H_2 elimination products $NiC_3H_6^+(X)$ for the 58 isotope; and intact adducts $NiC_3H_8^+$ for the 58, 60, 61, 62, and 64 isotopes. It appears that the detector is about a factor of 5 less sensitive to fast neutral C_3H_8 than to the Ni-containing cations.

It has not been possible to isolate and identify delayed H_2 elimination fragment ions, in part due to the complex Ni isotope pattern. We have succeeded in doing so for the $Co^+ + C_3H_8$ reaction, which produces a larger fraction of H_2, as will be described in a later publication.[34]

In Figure 4, we have normalized all mass spectra to give a constant ratio of prompt $NiC_2H_4^+$ intensity to the total intensity due to long-lived $NiC_3H_8^+$ and its fragmentation products. Since the retarding field slows ions down, we must be concerned with ion collection efficiency vs V_r. Integration of peak intensities vs V_r indicates that our collection efficiency for intact adduct ions remains constant within 20% for V_r up to 800 V. Collection efficiency for the Ni^+ fragments formed in region F1, the ions that traverse region R at the smallest speed, is constant within 20% for V_r up to 700 V.

3. Time-Resolved Branching Fractions. The experiment as carried out partitions the time t since complex formation into three overlapping windows. For $t_{ext} = 8$ μs, these are roughly $t = 2-10$ μs, $t = 6-24$ μs, and $t \geq 27$ μs. The earliest time window is the ion residence time in the source region, the time between the firing of the ionizing laser and the completion of ion acceleration, about $t_{ext} + 2$ μs. In this interval, we can measure an apparent *total reaction cross section* that includes as products long-lived complexes that survive extraction intact plus elimination products born prior to extraction. The time scale is somewhat fuzzy due to the *distribution* of times between initiation of a collision and ion extraction; some Ni^+ collide with C_3H_8 soon after the ionization pulse while others collide later. We can also measure the branching fractions of prompt CH_4 elimination products, prompt H_2 elimination products, and long-lived adducts averaged over the same time window by integrating the simple TOF-MS peaks. These data are collected in Table 1 for the two collision energies with $t_{ext} = 8$ μs. Those few complexes that fragment to elimination products *during* the 2 μs ion acceleration time will appear as small tails on the proper elimination fragment ion and will mostly be included in the correct channel. We are blind to complexes that return to $Ni^+ + C_3H_8$ during this first time window, since the peak from Ni^+ that never collides with C_3H_8 is enormous on the scale of products. Comparison of the rough estimate of the overall cross section to the Langevin cross section at 0.01 eV indicates that only about 35% of the $Ni^+ + C_3H_8$ collisions return to reactants on the time scale of $t = 2-10$ μs.

TABLE 3: $NiC_3H_8^+$ Fragmentation Pattern, $t = 6-24$ μs after Collision[a]

E_t (eV)	fraction dissoc	fragment branching		
		Ni^+	$NiC_2H_4^+$	$NiC_3H_6^+$
0.01	0.35	0.79 ± 0.20	0.17 ± 0.08	$\leq 0.04 \pm 0.03$[b]
0.21	0.75	0.79 ± 0.08	0.17 ± 0.06	$\leq 0.04 \pm 0.03$[b]

[a] Data for $t_{ext} = 8$ μs, $U_{ext} = 1280$ eV. Fragmentation of those ions that survive extraction as adducts but fragment before the retarding field, which places the time since initiation of $Ni^+ + C_3H_8$ collisions in the range 6−24 μs. [b] Upper bound only.

At nominal 0.01 eV and at 0.21 eV collision energy, most of the observed products sampled at $t = 2-10$ μs after initiation of a collision are *adducts*. For $E = 0.21$ eV, we can make a somewhat stronger statement based on the behavior of the mass spectrum vs t_{ext}. As t_{ext} increases from 1 to 8 μs, the three detected products 1a, 1b, and 1c grow *linearly*, and the *fraction* of elimination products remains *constant* within experimental uncertainty. This means that elimination occurs at a roughly constant *rate* over the entire range of times $t = 3-10$ μs following initiation of a collision. For t_{ext} below 1 μs, we continue to observe elimination products but they are increasingly badly contaminated by the high-energy background collisions that occur during ion extraction.

The middle time window is the time spent by complexes in field-free region F1 (Figure 2), prior to interrogation by the retarding fields in region R. For the typical value $U_{ext} = 1280$ eV, the flight time for $NiC_3H_8^+$ in F1 is 18 μs. Thus, for $t_{ext} = 8$ μs, complexes enter region R with t in the range 20−28 μs after the initiation of the collision. The 20 μs time corresponds to the latest-born complexes, and the 28 μs time corresponds to the earliest-born complexes. The retarding field device in effect integrates the decay kinetics of surviving complexes over a time window that varies from $t = 2-20$ μs (latest born) to $t = 10-28$ μs (earliest born). In paper 2, we will average the kinetics model appropriately to match what the experiment measures.

The heading of Table 3 describes this rather complicated averaging over the middle time window by using the midpoints of each interval, 6−24 μs. At both 0.01 and 0.21 eV collision energy, by far the predominant fragment ion formed at these "middle" times is Ni^+. We also detect a very small peak due to $NiC_2H_4^+ + CH_4$ fragments born in region F1. At 0.21 eV, it is barely visible in the spectrum for $V_r = 600$ V in Figure 4. The signal-to-noise ratio does not allow us to observe a small peak due to $NiC_3H_6^+ + H_2$, partly due to the small loss of mass in this channel. It is clear that the $NiC_3H_6^+$ fragment is substantially smaller than the $NiC_2H_4^+$ fragment; we set an upper bound on its intensity in Table 3. To estimate absolute branching fractions for the major decay channels of the complexes that fragment about 6−24 μs after formation, we assume the same 4:1 branching between CH_4 and H_2 elimination as occurred for prompt elimination at short times.

Table 3 gives the branching results for the middle time window. At both 0.01 and 0.21 eV, 79% of the fragmentation during the middle time window leads back to $Ni^+ + C_3H_8$ reactants and 17% leads to $NiC_2H_4^+ + CH_4$ elimination products, assuming one-fourth as many H_2 as CH_4 elimination products. However, the *time scale* of these processes is significantly different at 0.01 and 0.21 eV. At the lower collision energy of 0.01 eV, only 35% of the long-lived complexes that survive extraction fragment in region F1 (Table 3). At 0.21 eV, fully 75% of the long-lived complexes fragment in region F1.

If we assume *single-exponential decay* of the $NiC_3H_8^+$ complexes that survive extraction, we can use the fraction of complexes that fragment in region F1 to compute a crude, two-point estimate of the time constant of the metastable decay. The resulting lifetime estimates are 56 ± 25 μs at 0.01 eV and 17 ± 4 μs at 0.21 eV. These estimates are very rough due to the range of collision initiation times. We emphasize that the data do not preclude more complicated, nonexponential decay of the complexes, as will be found in the models of paper 2.

The third time window runs from the time the complexes exit the retarding region R to infinity. We can cleanly measure one additional quantity, the magnitude of the signal due to long-lived complexes that *have not yet fragmented* on exiting region R (Figure 2). The beginning of this time window depends only slightly on the retarding potential V_r. For $V_r = 600$ V and $U_{ext} = 1280$ eV, complexes spend 21 μs in F1 and R combined. For $t_{ext} = 8$ μs, this corresponds to $t = 23-31$ μs since initial complex formation. With $V_r = 600$ V, all fragments are sufficiently retarded that the $^{58}NiC_3H_8^+$ peak becomes sharp. Its intensity measures the number of adducts that survive *at least* 23−31 μs after formation. We measure this quantity most accurately as the ratio of the area under peak b to the area under the *prompt* $^{58}NiC_2H_4^+$ elimination peak, since both of these peaks should suffer comparably small losses with the retarding voltage quite high. This ratio is 1.0 ± 0.2 at 0.21 eV collision energy.

IV. Comparison with Earlier Work

The $Ni^+ + C_3H_8$ reaction has been studied in many different laboratories using ion beams and collision cells,[5−7,11,16] an ion-cyclotron-resonance mass spectrometer,[8,9] a tandem mass spectrometer,[16] a fast flow reactor at 0.75 Torr of He,[10] and now in our crossed-beam apparatus. Primarily based on modeling of the deuterium isotope effects on cross section and kinetic energy release distributions (KERDs), van Koppen et al.[16] inferred that the barrier to CH insertion is rate limiting and lies 0.10 ± 0.03 eV *below* reactants. Our crossed-beam study with carefully controlled reactant internal energy strongly suggests that a potential energy barrier lies very near the energy of $Ni^+(^2D_{5/2}) + C_3H_8$ reactants. In Figure 3, the apparent cross section for elimination products rises dramatically from nominal 0.01 to 0.21 eV collision energy. Ours is the only study to observe such an apparent energy threshold for formation of elimination products. The elimination cross-section data of Armentrout and co-workers[11,16] *decrease* smoothly from 0.05 to 1.0 eV. Our reactants have been drained of all electronic energy and most internal energy, and the merged beams access very low collision energies as well. The ability to discern the energy threshold is presumably closely related to these factors. In addition, our detection time scale of $t = 0-25$ μs is much shorter than that of Armentrout and co-workers, who detect products that have evolved as long as 500 μs at $E_t = 0.05$ eV.[35] On a longer time scale, many of our adducts may slowly evolve to elimination products. We will attempt to determine the threshold energy quantitatively by including such effects in the rate model of paper 2.

We also are able to observe the behavior of the long-lived $NiC_3H_8^+$ collision complexes under better defined conditions than in earlier work. In particular, the resonant ionization process ensures that our Ni^+ reactant is formed exclusively in the lowest energy spin−orbit level, $^2D_{5/2}$. Under these conditions, at nominal 0.01 eV collision energy we find that about 65% of the Langevin collisions form complexes that survive

several microseconds, long enough to be detected efficiently as adducts in our experiment. This population of long-lived complexes then fragments quite slowly, yielding 80% Ni^+ and 20% elimination products, including both CH_4 and H_2. If we combine the 20% branching into elimination products with the estimated total cross section $\sigma/\sigma_L = 0.65$ for forming detectable products (both adducts and elimination products), we estimate the elimination reaction efficiency $\sigma_{elim}/\sigma_L \approx 0.13$. This is the same as Armentrout's elimination reaction efficiency of 0.13 at 0.05 eV.[16]

At both collision energies, a striking feature of our data is the wide range of time scales over which elimination occurs. We observe elimination products throughout the observable time range, as early as $t = 0.5$ μs and as late as $t = 25$ μs. The primary effect of increasing the collision energy to 0.21 eV is more rapid fragmentation of the $NiC_3H_8^+$ complexes. At 0.01 eV, if the decay were exponential, our two-point sampling of the decay would yield a crude estimate of the time constant as $\tau(0.01\text{ eV}) \approx 60$ μs. At 0.21 eV, if the decay were exponential, the time constant would be $\tau(0.21\text{ eV}) \approx 17$ μs. However, we emphasize that the data are consistent with nonexponential decay at both energies.

Most of the early studies do not mention detection of the long-lived collision complexes that form the bulk of the products observed in this work. Tolbert and Beauchamp[36] reported 25% adduct ion products at $E = 0.5$ eV when colliding a Ni^+ beam with C_3H_8 gas in a collision cell at 1.5 mTorr. Tonkyn, Ronan, and Weisshaar[10] performed their work in a fast flow reactor under *multicollision* conditions at 0.75 Torr of He with a 300 K Boltzmann distribution of collision energies. They found 1.7% CH_4 elimination, 0.3% H_2 elimination, and 98% intact $NiC_3H_8^+$ parents, quite similar to our $t = 2-10$ μs branching results at 0.01 eV (Table 1). On the basis of a simple third-body stabilization kinetics model with the strong collision assumption, they deduced that the metastable $NiC_3H_8^+$ collision complex lived at least 1.4 μs. In an ion beam + collision cell experiment, Armentrout and co-workers[16] estimated the lifetime of complexes formed at collision energy $E_t = 0.05$ eV from the increase in $NiC_3H_8^+$ signal with propane pressure in the cell. From a Stern−Volmer model they obtained a lifetime of 3.8 μs, rather shorter than our two-point estimates of the lifetime at 0.21 eV and nominal 0.01 eV.

Most recently, van Koppen et al.[16] measured the kinetic energy release distributions (KERDs) of the metastable decay products from $NiC_3H_8^+$ parents. The $NiC_3H_8^+$ parent ions are gently extracted from an electron impact ionization source of Ni^+ containing 10^{-3} Torr of C_3H_8 at 300 K. They have spent 0−50 μs in the source region[37] and an additional 6−14 μs prior to fragmentation in the second field-free region of a tandem mass spectrometer.[16] Thus, the range of times since complex formation is roughly 6−64 μs. Analysis of the fragments reveals 56 ± 4% Ni^+, 28 ± 4% $NiC_2H_4^+$, and 16 ± 4% $NiC_3H_6^+$ (Table 3). This is a significantly higher yield of elimination fragments than we observe at either energy. van Koppen's complexes also make an unusually large percentage of H_2 elimination products compared with almost all other studies. The ratio of CH_4:H_2 elimination products is only 2:1 compared with 4:1 observed in many other techniques. It is probable that some of van Koppen's complexes suffer one or two stabilizing collisions in the source prior to extraction into high vacuum; i.e., single-collision conditions may not entirely prevail. Loss of substantial internal energy might help to shut off the return to $Ni^+ + C_3H_8$. We discuss these data in detail in Section V.C of paper 2.

A comprehensive model of this reaction must explain why the elimination branching is quite robust in the face of widely varying initial conditions. Earlier studies[5−11,16] vary widely in the distribution of collision energies, Ni^+ electronic states, and propane internal energy, as well as the background gas pressure and the time scale over which products are probed. Nevertheless, Table 2 shows close agreement on the branching between elimination products, $NiC_2H_4^+ + CH_4$ and $NiC_3H_6^+ + H_2$. Most studies find 80−85% CH_4 elimination.[5,8−10,16] The ion-beam studies of refs 6 and 7 found only 67% CH_4 elimination.

Finally, we comment that statistical models of complex decay as described in paper 2 and in ref 16 indicate that lifetimes, cross sections, and branching fractions are critically sensitive to the distribution of internal energy (electronic and vibrational) and orbital angular momentum in the complexes. The tandem mass spectrometer, ion beam plus gas cell, and our crossed-beam experiments probably do not match in internal energy. Aside from questions about collision energy, other Ni^+ sources can also produce excited electronic states. We showed explicitly in an earlier *J*-specific study of Fe^+ that additional spin−orbit energy enhanced the cross section with propane but not with *n*-butane,[21] as if the propane reaction were very near threshold. The current work suggests that even the excited spin−orbit level $Ni^+(^2D_{3/2})$ at 0.19 eV would have sufficient energy to substantially shorten the observed $NiC_3H_8^+$ complex lifetimes. Our alkane reactant is introduced by a supersonic pulsed valve. Vibrational temperatures of polyatomic molecules in neat supersonic expansions are ∼50 K.[29] Propane has vibrational frequencies ranging from 200 to 2967 cm^{-1}.[38] The Boltzmann distribution predicts that only 0.5% of propane molecules have 1 quantum of a 200 cm^{-1} vibration at 50 K. This excited fraction increases to 40% at 300 K. If experimental complex lifetimes are to be modeled meaningfully, it is very important to know as much as possible about the collisions that formed the complexes. We will describe the effect of modest amounts of internal energy on model lifetimes and fragmentation branching in detail in paper 2.

V. Conclusions

Our new data illustrate the potential of time-of-flight techniques for extracting detailed information about the time scale of an ion−molecule reaction using resonant two-photon ionization to form reactant ions promptly in time. Although we have carefully controlled the reaction conditions, it is clear that the $Ni^+ + C_3H_8$ reaction forms long-lived complexes that fragment over a wide range of time scales from 0.5 to 25 μs. Some of the complexes survive longer than 25 μs. Yet the branching fractions are quite similar at all times. We will show in paper 2 how a simple model involving parallel paths to H_2 and CH_4 elimination products can explain the broad range of time scales as arising from the effects of orbital angular momentum on complex lifetimes. Even when the collision energy and the internal electronic and vibrational energy are carefully controlled, complex lifetimes should vary over several decades when potential barriers lie within several kcal/mol of the reactant asymptotic energy. In future experimental work, a Reflectron analyzing electrostatic mirror or an ion trap might extend the observation time toward hundreds of microseconds as well.

Acknowledgment. J.C.W. thanks the National Science Foundation (CHE-9303918) and the donors of the Petroleum Research Foundation (PRF-31202-AC6) for generous support of this research. R.J.N. gratefully acknowledges support from

a Department of Education fellowship and a Procter and Gamble Fellowship. S.S.Y. acknowledges support from a Lubrizol Fellowship.

References and Notes

(1) Eller, K.; Schwarz, H. *Chem. Rev. (Washington, D.C.)* **1991**, *91*, 1121. Armentrout, P. B. In *Selective Hydrocarbon Activation: Principles and Progress*; Davies, J. A., Watson, P. L., Greenberg, A., Liebman, J. F., Eds.; VCH: New York, 1990. Beauchamp, J. L.; van Koppen, P. A. M. In *Energetics of Organometallic Species*; Martinho Simões, J. A., Ed.; Kluwer Academic Publishers: Dordrecht, 1992. Weisshaar, J. C. In *State-Selected and State-to-State Ion−Molecule Reaction Dynamics*; Ng, C. Y., Ed.; Wiley: New York, 1992. *Organometallic Ion Chemistry*; Freiser, B. S., Ed.; Kluwer Academic Publishers: Dordrecht, The Netherlands, 1996.

(2) Mitchell, S. A. In *Gas-Phase Metal Reactions*; Fontijn, A., Ed.; Elsevier: Amsterdam, 1992. Brown, C. E.; Mitchell, S. A.; Hackett, P. A. *J. Phys. Chem.* **1991**, *95*, 1062. Weisshaar, J. C. In *Laser Chemistry of Organometallics*; Chaiken, J., Ed.; American Chemical Society: Washington, DC, 1993.

(3) Bauschlicher, C. W.; Langhoff, S. R.; Partridge, H. In *Modern Electronic Structure Theory*; Yarkony, D. R., Ed.; World Scientific Publishing Company: London, 1995. Siegbahn, P. E. M.; Blomberg, M. R. A. *J. Am. Chem. Soc.* **1992**, *114*, 10548. Blomberg, M. R. A.; Siegbahn, P. E. M.; Svensson, M.; Wennerberg, J. In *Energetics of Organometallic Species*; Martinho Simões, J. A., Ed.; Kluwer Academic Publishers: Dordrecht, 1992. Musaev, D. G.; Morokuma, K.; Koga, N.; Nguyen, K. A.; Gordon, M. S.; Cundari, T. R. *J. Phys. Chem.* **1993**, *97*, 11435. Perry, J. K.; Ohanessian, G.; Goddard, W. A. *J. Phys. Chem.* **1993**, *97*, 5238.

(4) Armentrout, P. B.; Beauchamp, J. L. *J. Am. Chem. Soc.* **1981**, *103*, 784.

(5) Halle, L. F.; Armentrout, P. B.; Beauchamp, J. L. *Organometallics* **1982**, *1*, 963.

(6) Halle, L. F.; Houriet, R.; Kappes, M. M.; Staley, R. H.; Beauchamp, J. L. *J. Am. Chem. Soc.* **1982**, *104*, 6293.

(7) Houriet, R.; Halle, L. F.; Beauchamp, J. L. *Organometallics* **1983**, *2*, 1818.

(8) Jacobson, D. B.; Freiser, B. S. *J. Am. Chem. Soc.* **1983**, *105*, 736.

(9) Jacobson, D. B.; Freiser, B. S. *J. Am. Chem. Soc.* **1983**, *105*, 5197.

(10) Tonkyn, R.; Ronan, M.; Weisshaar, J. C. *J. Phys. Chem.* **1988**, *92*, 92.

(11) Georgiadis, R.; Fisher, E. R.; Armentrout, P. B. *J. Am. Chem. Soc.* **1989**, *111*, 4251.

(12) van Koppen, P. A. M.; Brodbelt-Lustig, J.; Bowers, M. T.; Dearden, D. V.; Beauchamp, J. L.; Fisher, E. R.; Armentrout, P. B. *J. Am. Chem. Soc.* **1990**, *112*, 5663.

(13) Schultz, R. H.; Armentrout, P. B. *J. Am. Chem. Soc.* **1991**, *113*, 729.

(14) van Koppen, P. A. M.; Brodbelt-Lustig, J.; Bowers, M. T.; Dearden, D. V.; Beauchamp, J. L.; Fisher, E. R.; Armentrout, P. B. *J. Am. Chem. Soc.* **1991**, *113*, 2359.

(15) van Koppen, P. A. M.; Kemper, P. R.; Bowers, M. T. *J. Am. Chem. Soc.* **1992**, *114*, 10941.

(16) van Koppen, P. A. M.; Bowers, M. T.; Fisher, E. R.; Armentrout, P. B. *J. Am. Chem. Soc.* **1994**, *116*, 3780.

(17) Haynes, C. L.; Fisher, E. R.; Armentrout, P. B. *J. Phys. Chem.* **1996**, *100*, 18300.

(18) Holthausen, M. C.; Fiedler, A.; Schwarz, H.; Koch, W. *J. Phys. Chem.* **1996**, *100*, 6236. Holthausen, M. C.; Koch, W. *J. Am. Chem. Soc.* **1996**, *118*, 9932. Holthausen, M. C.; Koch, W. *Helv. Chim. Acta* **1996**, *79*, 1939.

(19) Yi, S. S; Blomberg, M. R. A.; Siegbahn, P. E. M.; Weisshaar, J. C. *J. Phys. Chem. A* **1998**, *102*, XXXX (accompanying paper 2).

(20) Sanders, L.; Hanton, S. D.; Weisshaar, J. C. *J. Chem. Phys.* **1990**, *92*, 3498. Noll, R. J.; Weisshaar, J. C. *J. Am. Chem. Soc.* **1994**, *116*, 10288.

(21) Hanton, S. D.; Noll, R. J.; Weisshaar, J. C. *J. Phys. Chem.* **1990**, *94*, 5655. Hanton, S. D.; Noll, R. J.; Weisshaar, J. C. *J. Chem. Phys.* **1992**, *96*, 5176.

(22) Noll, R. J. Doctoral Dissertation, University of Wisconsins−Madison, 1994.

(23) Hunt, W. W.; Huffman, R. E.; McGee, K. E. *Rev. Sci. Instrum.* **1964**, *35*, 82. Hunt, W. W.; Huffman, R. E.; Saari, J.; Wassel, G.; Betts, J. F.; Paufve, E. H.; Wyess, W.; Fluegge, R. A. *Rev. Sci. Instrum.* **1964**, *35*, 88. Ferguson, R. E.; McCulloh, K. E.; Rosenstock, H. M. *J. Chem. Phys.* **1965**, *42*, 100. Dugger, D. L.; Kiser, R. W. *J. Chem. Phys.* **1967**, *47*, 5054.

(24) Robinson, P. J.; Holbrook, K. A. *Unimolecular Reactions*; Wiley-Interscience: New York, 1972. Gilbert, R. G.; Smith, S. C. *Theory of Unimolecular and Recombination Reactions*; Blackwell Scientific Publications: Oxford, UK, 1990. Aubanel, E. E.; Wardlaw, D. M.; Zhu, L.; Hase, W. L. *Int. Rev. Phys. Chem.* **1991**, *10*, 249. Baer, T.; Hase, W. L. *Unimolecular Reaction Dynamics*; Oxford University Press: New York, 1996.

(25) Morse, M. D.; Hopkins, J. B.; Langridge-Smith, P. R. R.; Smalley, R. E. *J. Chem. Phys.* **1983**, *79*, 5316. Powers, D. E.; Hansen, S. G.; Geusic, M. E.; Michalopoulos, D. L.; Smalley, R. E. *J. Chem. Phys.* **1983**, *78*, 2866.

(26) Sugar, J.; Corliss, C. *J. Phys. Chem. Ref. Data* **1985**, *14* (Suppl. 2). Fuhr, J. R.; Martin, G. A.; Wiese, W. L. *J. Phys. Chem. Ref. Data* **1988**, *17* (Suppl. 4).

(27) Page, R. H.; Gudeman, C. S. *J. Opt. Soc. Am.* **1990**, *B7*, 1761.

(28) Wiley, W. C.; McLaren, I. H. *Rev. Sci. Instrum.* **1955**, *26*, 1150.

(29) Gallagher, R. J. Doctoral Dissertation, Yale University, 1972.

(30) Cooper, G.; Zheng, Y.; Burton, G. R.; Brion, C. E. *Rev. Sci. Instrum.* **1993**, *64*, 1140.

(31) *CRC Handbook of Chemistry and Physics*; 75th ed.; Lide, D. R., Ed.; CRC Press: Boca Raton, FL, 1995.

(32) Gioumousis, G.; Stevenson, D. P. *J. Chem. Phys.* **1958**, *29*, 294.

(33) Noll, R. J.; Weisshaar, J. C. Unpublished results.

(34) Yi, S. S.; Noll, R. J.; Weisshaar, J. C. Manuscript in preparation.

(35) Estimated from the experimental flight path. The experimental time window depends on the kinetic energies of ions and it is roughly 100 μs for energies near 1 eV. See: Ervin, K. M.; Armentrout, P. B. *J. Chem. Phys.* **1985**, *83*, 166.

(36) Tolbert, M. A.; Beauchamp, J. L. *J. Am. Chem. Soc.* **1986**, *108*, 7509.

(37) van Koppen, P. A. M. Personal communication.

(38) Shimanouchi, T. *Tables of Molecular Vibrational Frequencies*; National Bureau of Standards: Washington, DC, 1972.